



## *reciprocalspaceship*: a Python library for crystallographic data analysis

Jack B. Greisman, Kevin M. Dalton and Doeke R. Hekstra

*J. Appl. Cryst.* (2021). **54**, 1521–1529



**IUCr Journals**  
CRYSTALLOGRAPHY JOURNALS ONLINE

Author(s) of this article may load this reprint on their own web site or institutional repository provided that this cover page is retained. Republication of this article or its storage in electronic databases other than as specified above is not permitted without prior permission in writing from the IUCr.

For further information see <https://journals.iucr.org/services/authorrights.html>



# *reciprocalspaceship*: a Python library for crystallographic data analysis

Jack B. Greisman,<sup>a</sup> Kevin M. Dalton<sup>a</sup> and Doeke R. Hekstra<sup>a,b\*</sup>

<sup>a</sup>Department of Molecular and Cellular Biology, Harvard University, 52 Oxford Street, Cambridge, MA 02138, USA, and

<sup>b</sup>John A. Paulson School of Engineering and Applied Sciences, Harvard University, Cambridge, Massachusetts, USA.

\*Correspondence e-mail: doeke\_hekstra@harvard.edu

Received 21 April 2021

Accepted 23 July 2021

Edited by S. Boutet, SLAC National Accelerator Laboratory, Menlo Park, USA

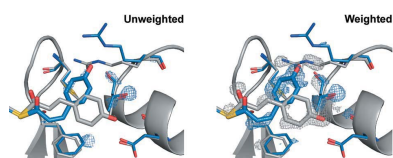
**Keywords:** X-ray crystallography; data analysis; Python.

Crystallography uses the diffraction of X-rays, electrons or neutrons by crystals to provide invaluable data on the atomic structure of matter, from single atoms to ribosomes. Much of crystallography's success is due to the software packages developed to enable automated processing of diffraction data. However, the analysis of unconventional diffraction experiments can still pose significant challenges – many existing programs are closed source, sparsely documented, or challenging to integrate with modern libraries for scientific computing and machine learning. Described here is *reciprocalspaceship*, a Python library for exploring reciprocal space. It provides a tabular representation for reflection data from diffraction experiments that extends the widely used *pandas* library with built-in methods for handling space groups, unit cells and symmetry-based operations. As is illustrated, this library facilitates new modes of exploratory data analysis while supporting the prototyping, development and release of new methods.

## 1. Introduction

The analysis of most diffraction experiments begins with processing diffraction images and ends with refining an atomic model that is consistent with the observed data in order to answer a scientific question. Numerous software suites and command-line applications address different stages of the processing pipeline and these diverse programs are typically combined to address the challenges of a particular data set (Adams *et al.*, 2010; Winn *et al.*, 2011; Winter *et al.*, 2018; Grosse-Kunstleve *et al.*, 2002; Kabsch, 2010*a,b*; Otwinowski & Minor, 1997). However, many novel diffraction experiments do not fit easily into the processing pipelines established within existing crystallographic software. Such experiments often require custom scripts and programs to analyze the resulting data. Recent examples of such experiments include time-resolved pump–probe experiments that investigate the structural dynamics within room-temperature crystals (Hekstra *et al.*, 2016; Dods *et al.*, 2021; Wickstrand *et al.*, 2020) and new approaches to phasing (Garcia-Bonete & Katona, 2019; Hatti *et al.*, 2021). New software is needed to facilitate such custom analyses and improve the development, reproducibility and adoption of novel diffraction experiments.

A software library supporting such experiments must provide built-in methods to handle space groups, unit cells and symmetry operations. This first requirement is met by several crystallographic libraries for Python, including the *Computational Crystallography Toolbox (CCTBX)* (Grosse-Kunstleve *et al.*, 2002) and *GEMMI* (Wojdyr, 2021). However, in our experience, exploratory analysis of reflection data and the development of new analysis methods would, in addition, greatly benefit from seamless integration with existing



```
In [1]: import reciprocalspaceship as rs
In [2]: dataset = rs.read_mtz("HEWL_SSAD_24IDC.mtz")
In [3]: dataset.cell
Out[3]: <gemmi.UnitCell(79.3435, 79.3435, 37.8098, 90, 90, 90)>
In [4]: dataset.spacegroup
Out[4]: <gemmi.SpaceGroup("P 43 21 2")>
In [5]: dataset.sample(5)
Out[5]:
```

	FreeR_flag	IMEAN	SIGMEAN	I(+)	SIGI(+)	I(-)	SIGI(-)	N(+)	N(-)
<b>H K L</b>									
<b>39 14 5</b>	5	76.448586	2.5888965	78.261024	3.6358812	74.58466	3.6871622	12	12
<b>23 16 8</b>	8	349.9014	5.072093	341.31744	7.1655827	358.5211	7.1804857	40	40
<b>19 4 2</b>	11	3038.7883	38.110188	2993.984	53.89258	3083.6042	53.899307	56	56
<b>24 10 0</b>	15	53.134754	1.0403585	53.134754	1.0403585	53.134754	1.0403585	46	46
<b>29 23 1</b>	4	474.38315	11.350164	454.9555	16.014786	493.99023	16.08858	16	16

**Figure 1**  
A screenshot demonstrating the use of *reciprocalspaceship* in a Jupyter notebook. `DataSet` objects can be used to represent reflection data with associated unit-cell and space-group information.

scientific computing software, including *NumPy* (Harris *et al.*, 2020) and *SciPy* (Virtanen *et al.*, 2020). This requirement is not met by the existing libraries, which use internal data structures that are not directly compatible with *NumPy*. As we show here, meeting this additional requirement enables crystallographers to deploy the rich arsenal of data analysis, statistics and machine-learning tools developed across other disciplines.

Key to such integration with scientific Python software is the observation that crystallographic data are inherently tabular due to Bragg’s law, with each observed reflection described by a Miller index. This property underlies many of the file formats for storing diffraction data: integrated intensities and any reflection-specific metadata are typically stored with the associated Miller index (see Fig. 1). For analysis in Python, tabular data are commonly represented using the *pandas* software library (Reback *et al.*, 2021). `pandas.DataFrame` objects provide support for the arbitrary manipulation of tabular data, storage of heterogeneous data types, and easy integration with any scientific computing or machine-learning library that supports *NumPy* arrays (Harris *et al.*, 2020).

Because of the tabular nature of crystallographic data and the widespread use of *pandas* in data science, we sought to develop a library that extends the `DataFrame` for reflection data by providing built-in support for space groups, unit cells and symmetry operations. This library, *reciprocalspaceship*, can be used to inspect reflection data, to develop new crystallographic methods and to release reproducible analysis pipelines for diffraction experiments. By embracing the norms for data science in Python, *reciprocalspaceship* will enable the development of new methods by the next generation of crystallographers.

## 2. *reciprocalspaceship* library

### 2.1. Mission statement

*reciprocalspaceship* is a free and open-source software library with the primary goal of simplifying the analysis of

crystallographic data in Python. To achieve this goal, we sought to design a software library that is intuitive for both crystallographers and Python programmers. This requires full support for common crystallographic operations, as well as easy integration with the scientific computing and machine-learning libraries that are developed and maintained by the Python community.

### 2.2. Design

The `DataFrame` is the core abstraction in *pandas*. *reciprocalspaceship* provides a `DataSet` class which extends the `DataFrame`, augmenting it to represent reflection data from diffraction experiments. `DataSet` objects store reflection data along with the associated space group and unit cell, and can be initialized from common reflection file formats such as MTZ files (Fig. 1). By extending the *pandas* `DataFrame`, it is possible to preserve its core functionality while adding built-in methods to support common crystallographic operations. These operations use the *GEMMI* library to represent space groups and unit cells (Wojdyr, 2021) and have been vectorized to increase performance.

This design allows *reciprocalspaceship* to complement the functionality of libraries such as *GEMMI* by providing data scientists familiar with the Python scientific computing ecosystem with an interface to reflection data that meets their expectations. In this way, *reciprocalspaceship* helps experts from other fields bring their perspectives and machine-learning tools to crystallography.

Furthermore, this library supports the use of MTZ files, allowing users to interface easily with existing and widely used computational crystallography infrastructure, such as *CCTBX* (Grosse-Kunstleve *et al.*, 2002), *CCP4* (Winn *et al.*, 2011) and *PHENIX* (Adams *et al.*, 2010). To support compatibility with MTZ files, *reciprocalspaceship* provides custom data types to represent different crystallographic data, such as intensities, structure factor amplitudes or phases. To ensure compatibility with other Python libraries, these data types are all represented internally using *NumPy* arrays of either 32-bit integer or floating-point values. Methods are also provided for inferring relevant data types based on standard MTZ column labels used to describe the data. `DataSet` objects can, moreover, contain any data type supported by *pandas*, including generic Python objects.

### 2.3. Features

The primary capabilities of this library are provided through the `DataSet` object, which builds on the core features of the *pandas* `DataFrame` to provide crystallographic support. `DataSet` objects can represent both merged and unmerged reflection data and provide the attributes and methods that are summarized in Table 1.

In addition to the `DataSet` object, *reciprocalspaceship* provides several algorithms that can be used for analysis. These include `merge()`, which implements the averaging of unmerged reflection data using maximum-likelihood weights, and `scale_merged_intensities()`, which implements

**Table 1**  
Core features of `reciprocalsspaceship.DataSet` objects.

<b>Attributes</b>	
<code>cell</code>	Unit-cell parameters
<code>spacegroup</code>	Space-group information
<code>merged</code>	Identifier for merged/unmerged data
<code>acentrics</code>	Access acentric reflections in <code>DataSet</code>
<code>centrics</code>	Access centric reflections in <code>DataSet</code>
<b>Methods</b>	
<b>(i) Input/Output</b>	
<code>from_gemmi()</code>	Create <code>DataSet</code> object from <code>gemmi.Mtz</code>
<code>to_gemmi()</code>	Create <code>gemmi.Mtz</code> object from <code>DataSet</code>
<code>write_mtz()</code>	Write <code>DataSet</code> to an MTZ file
<b>(ii) Symmetry</b>	
<code>apply_symop()</code>	Apply symmetry operation to reflections in <code>DataSet</code>
<code>expand_anomalous()</code>	Expand data by applying Friedel operator ( $\bar{h}, \bar{k}, \bar{l}$ )
<code>expand_to_pl()</code>	Generate all symmetrically equivalent reflections
<code>hkl_to_asu()</code>	Map reflections to reciprocal-space asymmetric unit
<code>hkl_to_observed()</code>	Map reflections to observed Miller indices
<b>(iii) Annotation</b>	
<code>compute_dHKL()</code>	Compute the real-space resolution of each reflection
<code>compute_multiplicity()</code>	Compute the multiplicity of each reflection
<code>label_absences()</code>	Label systematically absent reflections
<code>label_centrics()</code>	Label centric reflections
<b>(iv) Reshaping</b>	
<code>stack_anomalous()</code>	Convert anomalous data from two- to one-column format
<code>to_reciprocalgrid()</code>	Convert reflection data to 3D array populated at Miller indices
<code>unstack_anomalous()</code>	Convert anomalous data from one- to two-column format
<b>(v) Utilities</b>	
<code>assign_resolution_bins()</code>	Assign reflections in <code>DataSet</code> to resolution bins
<code>canonicalize_phases()</code>	Canonicalize all phase data to fall between $[-180, 180)$ degrees
<code>infer_mtz_dtypes()</code>	Infer MTZ dtypes from column names and underlying data

the French–Wilson algorithm to account for negative merged intensities (French & Wilson, 1978). These implementations can serve as templates for the development of new analysis methods using *reciprocalsspaceship*. The set of algorithms offered through this library will continue to expand as users implement new analyses intended for broader adoption.

#### 2.4. Development and documentation

*reciprocalsspaceship* is maintained on GitHub under a permissive MIT license in order to foster community involvement in its development, testing and documentation. Every change to the source code is assessed using an automated testing suite in order to support continuous integration (Krekel *et al.*, 2020). *reciprocalsspaceship* is available through

the *Python Package Index* (PyPI; <https://pypi.org/>) and can be installed on most systems using *pip*. Documentation is automatically generated from the *reciprocalsspaceship* GitHub repository to ensure up-to-date information is available for users. The website includes a User Guide section describing the design and features of *reciprocalsspaceship* and examples that use the library for crystallographic applications. The documentation also includes a guide for developers to support users who wish to contribute new features or methods to the library. By committing to an open-source development model, it will be possible to maintain this library to meet the evolving needs of crystallographers.

### 3. Examples

The following examples demonstrate the use of *reciprocalsspaceship* in the analysis of crystallographic data. These examples cover the merging of scaled observed intensities, analyzing anomalous differences from a single-wavelength anomalous dispersion (SAD) experiment and applying weights to a time-resolved difference map. These examples are intended to illustrate the breadth of crystallographic problems that can be addressed using this library, as well as its seamless integration with common scientific computing libraries. The examples are available as interactive Jupyter notebooks (Kluyver *et al.*, 2016) in the *reciprocalsspaceship* documentation (<https://hekstra-lab.github.io/reciprocalsspaceship/userguide/examples.html>).

#### 3.1. Assessing uncertainty in merging statistics

Merging statistics are useful for assessing the internal consistency of a data set and many different metrics have been proposed over the years (Weiss, 2001; Karplus & Diederichs, 2012). Although merging statistics are commonly reported by data reduction pipelines, they are often not reported with uncertainties and do not always give access to their underlying parameters, such as the number of resolution bins or the type of correlation coefficients to report. By facilitating inspection of the underlying reflection data, *reciprocalsspaceship* can be used to write quality control scripts to automate analysis pipelines or, as shown here, for use in the exploratory analysis of the properties of a single data set. By enabling crystallographers to try new statistical routines, *reciprocalsspaceship* may help in the development of more robust indicators of data quality.

To illustrate this, we computed  $CC_{1/2}$  and  $CC_{anom}$  for scaled unmerged reflection data. The data were collected at 6.5 keV on a tetragonal crystal of hen egg-white lysozyme at ambient temperature. The integrated intensities were scaled in *AIMLESS* and the data contain sufficient anomalous signal from the native sulfur atoms to determine experimental phases by the SAD method (Greisman *et al.*, 2021; Adams *et al.*, 2010; Evans & Murshudov, 2013; Terwilliger *et al.*, 2009). Using *reciprocalsspaceship*, it is possible to implement a function that merges redundant observations using inverse-variance weights [Fig. 2(a)]. This code takes advantage of the

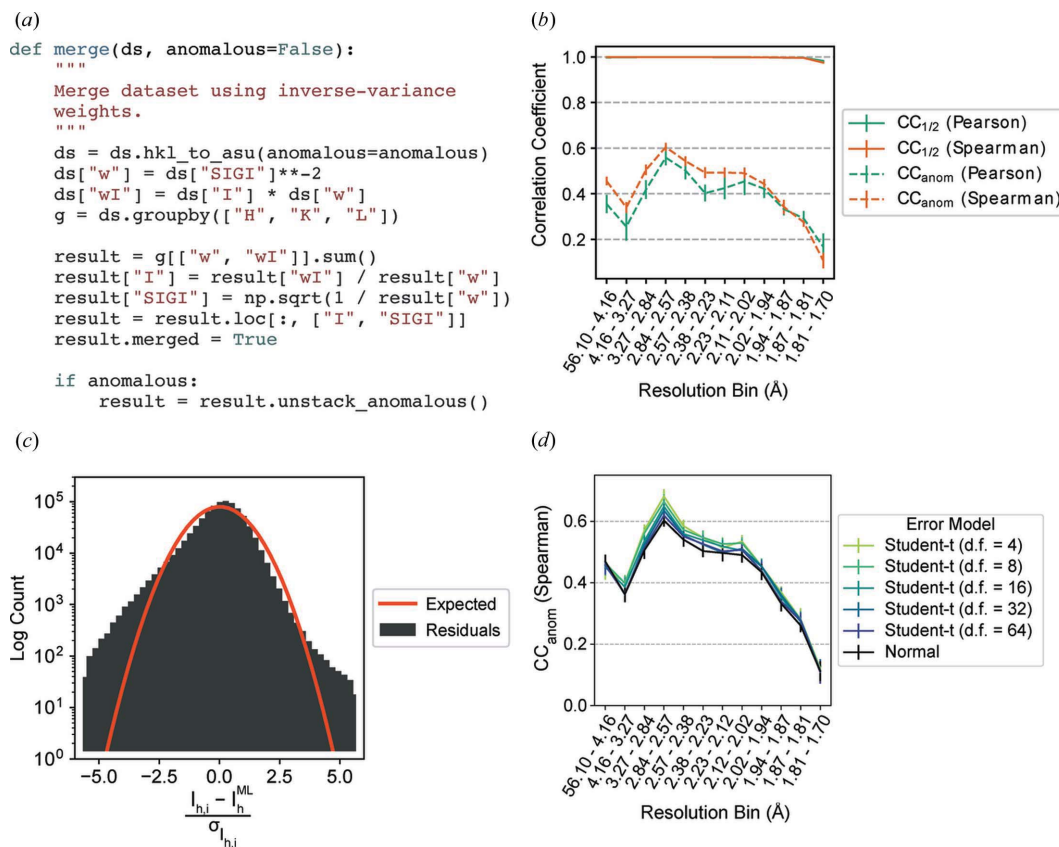


**Figure 2** Merging statistics for a hen egg-white lysozyme sulfur SAD data set. (a) The Python function for applying inverse-variance weights to obtain maximum-likelihood merged intensity estimates using *reciprocalspaceship*. (b) Correlation coefficients,  $CC_{1/2}$  and  $CC_{anom}$ , from repeated twofold cross validation. The Pearson  $CC_{anom}$  is more affected by outlier measurements in low- and intermediate-resolution bins than the Spearman  $CC_{anom}$ . (c) The distribution of residuals from observed intensities differs from the expected distribution of residuals for normally distributed observations. (d)  $CC_{anom}$  from twofold cross validation using Student  $t$ -distributed error models with varying degrees of freedom (d.f.). Error models with heavier tails show improvements in  $CC_{anom}$ . Error bars depict the mean  $\pm$  standard deviation from 15 repeats of twofold cross validation.

`groupby()` functionality inherited from *pandas* to perform calculations efficiently on a per-reflection basis (Reback *et al.*, 2021). By partitioning the observed reflections by image, this function can be used to merge different sets of observations independently for computing  $CC_{1/2}$  and  $CC_{anom}$ . Due to the modularity of this workflow, it is possible to repeat the random partitioning of observations by image to generate uncertainty estimates and to repeat these calculations using both Pearson and Spearman correlation coefficients.

As shown in Fig. 2(b), high  $CC_{1/2}$  values indicate that the resolution was limited by the experimental geometry rather than the crystal quality, which is common for data collected at low energy on strongly diffracting crystals. The  $CC_{anom}$  values show that significant anomalous signal was obtained up to the highest resolution bin. Furthermore, the Spearman correlation coefficients are systematically higher and have smaller uncertainties in the low- and intermediate-resolution ranges, indicating the presence of outliers in the data.

### 3.2. Merging observations with a robust error model

The difference observed for  $CC_{anom}$  between the Pearson and Spearman correlation coefficients in Fig. 2(b) suggests the

presence of outlier observations, despite the outlier rejection applied by *AIMLESS* (Evans & Murshudov, 2013). Since *AIMLESS* assumes a normally distributed error model for its observations, such outliers can have a large impact on estimates of the true merged intensity. We can evaluate whether a normally distributed error model is appropriate on the basis of the distribution of residuals between the observed intensities and the estimate of the true mean (Abrahams & Keve, 1971; Howell & Smith, 1992). This histogram can be made in just a few lines of Python by taking advantage of the *pandas* indexing approach [Fig. 2(c)]. Compared with the expected residuals for normally distributed observations, this data set has significantly heavier tails, with many observations several standard deviations away from the merged intensity.

The residuals in Fig. 2(c) suggest that merging may be improved by a more robust error model that can tolerate outliers. One popular choice of robust error model is the Student  $t$  distribution (Lange *et al.*, 1989). This distribution is parameterized by a location, a scale and the number of degrees of freedom,  $\nu$ , which controls the probability of large deviations from the mean. Importantly, the distribution approaches the normal distribution as  $\nu$  approaches infinity. Unlike the normal distribution, though, there is no analytical

expression for the maximum-likelihood estimator of the true mean given a set of observations under a Student  $t$ -distributed error model. However, we can construct an optimization problem to recover maximum-likelihood estimates of the merged intensity for each Miller index. To begin, we write the likelihood function, which is the probability of the data as a function of the mean intensity for each Miller index,  $h$ ,

$$P(\text{data} \mid \text{model}) = \prod_{h,i} P(I_{h,i} \mid \mu_h, \sigma_{I_{h,i}}). \quad (1)$$

This likelihood function asserts that the observed intensity  $I_{h,i}$ , for each Miller index  $h$  and observation  $i$ , is drawn from a distribution centered at the merged intensity  $\mu_h$ , with a scale determined by the empirical standard deviation of the observation,  $\sigma_{I_{h,i}}$ :

$$I_{h,i} \simeq P(\mu_h, \sigma_{I_{h,i}}). \quad (2)$$

To recover maximum-likelihood estimates of the intensities  $\hat{\mu}$ , we need only maximize equation (1) with respect to the merged intensities. Equivalently, we may minimize the negative logarithm of the likelihood  $\mathcal{L}$  with respect to the merged intensities as follows:

$$\begin{aligned} \mathcal{L} &= -\log P(\text{data} \mid \text{model}) \\ &= -\sum_{h,i} \log P(I_{h,i} \mid \mu_h, \sigma_{I_{h,i}}), \\ \hat{\mu} &= \operatorname{argmin}_{\mu} \left[ -\sum_{h,i} \log P(I_{h,i} \mid \mu_h, \sigma_{I_{h,i}}) \right], \end{aligned} \quad (3)$$

which has the advantage of converting a numerically unstable product into a sum.

This optimization was implemented in *PyTorch* (Paszke *et al.*, 2019) in a general form that could flexibly accept any probability distribution from the location-scale family as its error model (Paszke *et al.*, 2019). As an example, we merged the data under a Student  $t$ -distributed error model with varying degrees of freedom. The resulting  $\text{CC}_{\text{anom}}$  were compared with the normally distributed error model. The error models with fewer degrees of freedom outperformed the error models with more degrees of freedom, with the performance of the latter converging towards that of the normally distributed error model [Fig. 2(d)], consistent with the Student  $t$  distribution's approach towards a normal distribution with increasing degrees of freedom.

This example demonstrates the use of *reciprocalspaceship* to construct a flexible merging function using a machine-learning library. This greatly reduces the overhead required to prototype a new analysis method by making it easy to use existing and well supported libraries. Furthermore, the benefit of using robust statistical estimators, as demonstrated by the improved  $\text{CC}_{\text{anom}}$  values in Figs. 2(b) and 2(d), could readily extend to more complex procedures for scaling and merging anomalous data [e.g. as described by Terwilliger *et al.* (2016)] and suggests new avenues for improving the existing crystallographic analysis infrastructure. One such project, *careless*, combines *reciprocalspaceship* with *TensorFlow* to apply approximate Bayesian inference to new scaling and merging routines (Dalton *et al.*, 2021; Abadi *et al.*, 2015).

### 3.3. Revisiting the French–Wilson algorithm

In the previous example, we identified anomalous differences from a room-temperature sulfur SAD experiment. Here, we will examine this anomalous signal in real space by making an anomalous difference map. Before we can make a map, we need to correct the merged intensities to account for any negative values that may result from background subtraction during integration. This is commonly handled using a Bayesian approach first proposed by French and Wilson to estimate the true intensities  $J_h$  from the merged intensities  $I_h$  following data reduction (French & Wilson, 1978). Briefly, this algorithm determines posterior estimates for the true intensities  $\langle J_h \rangle$  by solving an integral,

$$\langle J_h \rangle = \int_0^{\infty} J_h \mathcal{N}(I_h \mid J_h, \sigma_{I_h}) P(J_h) dJ_h, \quad (4)$$

where the likelihood  $\mathcal{N}(I_h \mid J_h, \sigma_{I_h})$  is taken to be normally distributed, with the empirical error estimates for the merged intensities  $\sigma_{I_h}$  as standard deviations. The prior distribution  $P(J_h)$  is the Wilson distribution (Wilson, 1949):

$$P(J_h) = \begin{cases} \Sigma^{-1} \exp(-J_h/\Sigma) & J \geq 0, \text{ acentric,} \\ (2\pi\Sigma J_h)^{-1/2} \exp(-J_h/2\Sigma) & J \geq 0, \text{ centric,} \\ 0 & J < 0, \end{cases} \quad (5)$$

which is parameterized by  $\Sigma$ , the mean intensity of reflections at the appropriate resolution. To estimate  $\Sigma$  for each reflection, the classic French–Wilson algorithm computes the mean intensity of reflections in resolution shells and interpolates the mean values from shells adjacent to the particular reflection. Since the functional form of the prior distribution has strictly positive support (Wilson, 1949), the expectations computed from equation (4) are necessarily positive. Furthermore, the posterior structure factor amplitudes can be estimated as part of the same subroutine using the following integral:

$$\langle F_h \rangle = \int_0^{\infty} (J_h)^{1/2} \mathcal{N}(I_h \mid J_h, \sigma_{I_h}) P(J_h) dJ_h. \quad (6)$$

The implementation of this method in *reciprocalspaceship* differs significantly from the classical one, which was limited by the computing resources and statistical tools available at the time. Notably, rather than computing mean values in shells, we use a Gaussian smoother (Murphy, 2012) to regress the mean of the intensity distributions  $\Sigma$  against resolution. This regression model is quite flexible and offers an anisotropic mode which estimates the mean intensity locally as a function of the Miller indices. Whereas the original paper computed the posterior by interpolating a table of cached results (French & Wilson, 1978), our implementation uses Chebyshev–Gauss quadrature to evaluate the integrals efficiently on the fly. We generate quadrature points and weights with *NumPy* (Harris *et al.*, 2020) and compute the relevant log probabilities using the distribution classes implemented in *SciPy* (Virtanen *et al.*, 2020). Our implementation is tested for consistency with the original paper (French & Wilson, 1978) and with *CCTBX* (Grosse-Kunstleve *et al.*, 2002).

The merged intensities from the sulfur SAD experiment were rescaled using the French–Wilson algorithm and converted to structure factor amplitudes. This operation leaves large intensities relatively unchanged, while ensuring that any negative values become strictly positive [Fig. 3(a)]. Anomalous differences of the structure factor amplitudes were computed between Friedel pairs. The anomalous difference map shown in Fig. 3(b) was then constructed using phases derived from the refined model (PDB entry 7l84; J. B. Greisman, K. M. Dalton & D. R. Hekstra, to be published). The map shows significant anomalous peaks at a  $5\sigma$  contour, with the density strictly localized to each of the ten sulfur atoms in the lysozyme structure.

### 3.4. Identifying anomalous scattering atoms in real space

The anomalous difference map shown in Fig. 3(b) was made from the anomalous difference amplitudes and phases. It is

also possible to compute a real-space map using *reciprocal-spaceship* and *NumPy*, which enables one to use image processing software to automate the identification of anomalous scattering atoms. This process is illustrated in Fig. 3(c). The provided code snippet arranges the complex anomalous structure factors on a reciprocal-space grid and then computes the real-space anomalous difference map using the fast Fourier transform function (Cooley & Tukey, 1965) in *NumPy*. *scikit-image*, an image processing library (van der Walt *et al.*, 2014), can be used to identify peaks in the map. The automatically identified sites are overlaid with the anomalous difference map in Fig. 3(d), demonstrating that this procedure successfully identifies the 80 sulfur sites in the tetragonal lysozyme unit cell (ten sulfurs per copy, eight copies)

This example illustrates the use of *reciprocal-spaceship* to produce real-space maps from structure factors. Importantly, due to the seamless integration with *NumPy*, one can take advantage of Python image processing libraries to identify

peaks in the real-space density. Due to the wealth of libraries and tools written by the Python community, this feature of *reciprocal-spaceship* can provide the opportunity to develop and test new algorithms rapidly and to expand the crystallographic community by providing data science tools familiar to researchers from many other fields. In this manner, the use of *reciprocal-spaceship* could simplify existing data processing pipelines and perhaps be useful in the development of new methods in crystallographic data analysis or structural bioinformatics.

### 3.5. Applying weights to a time-resolved difference map

Time-resolved crystallography experiments make use of X-ray diffraction to monitor structural changes in a crystalline sample. Commonly, structural changes are initially evaluated on the basis of isomorphous difference maps. Such maps are computed by estimating the difference in structure factor amplitudes of the sample before and after a perturbation. Difference maps are often noisy due to systematic errors or scaling artifacts and are frequently weighted by the magnitude of the difference signal and/or the error estimates associated with the empirical differences in structure factor amplitudes. In this example we will

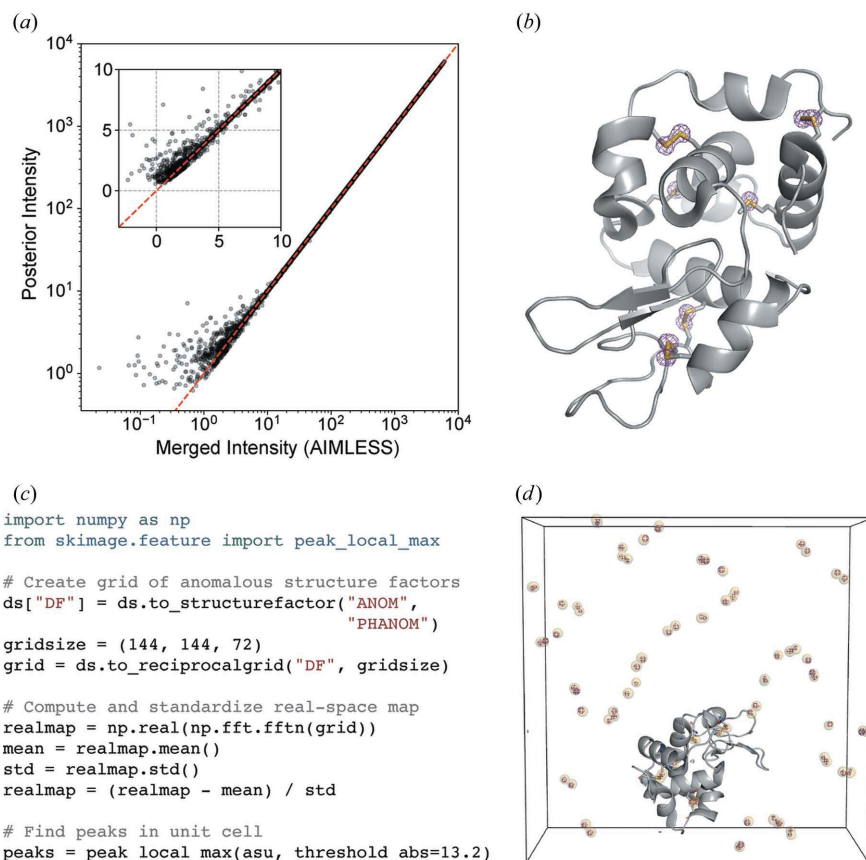


**Figure 3**

Analysis of anomalous differences from a sulfur SAD experiment. (a) Application of the French–Wilson algorithm to merged intensities. Large intensities are relatively unchanged, while small and negative intensities are corrected to be strictly positive. The red dashed line shows  $y = x$  and the inset highlights the small and negative merged intensities. (b) An anomalous difference map using difference structure factor amplitudes derived from the room-temperature sulfur SAD data set and phases from the refined model (PDB 7l84). The map is contoured at  $5\sigma$ . (c) Example code for identifying anomalous scattering sites in an anomalous difference map. (d) The unit cell containing sulfur sites identified using the code snippet (yellow spheres), overlaid with the anomalous difference map (purple mesh, contoured at  $10\sigma$ ). The protein molecule from one asymmetric unit of PDB 7l84 is shown in gray. The images in (b) and (d) were rendered using *PyMOL* (Schrödinger, 2020).

visualize the effects of applying weights to a time-resolved difference map of photoactive yellow protein (PYP). PYP is a model system in time-resolved crystallography based on the *trans*-to-*cis* isomerization of its 4-hydroxycinnamyl chromophore upon absorption of blue light (Genick *et al.*, 1997). This data set was collected at the BioCARS Laue beamline APS-14-ID and comprises matched images collected in the dark and 2 ms after illumination with blue light. These data were collected and provided by Marius Schmidt and Vukica Šrajer.

Several schemes have been used to apply weights to time-resolved difference maps. Many of them take the form of equation (7), involving a term based on the squared uncertainty in the difference structure factor amplitude ( $\sigma_{\Delta F}^2$ ) and its observed mean over reflections ( $\overline{\sigma_{\Delta F}^2}$ ) and, optionally, a scale term based on the squared magnitude of the observed difference structure factor amplitude ( $|\Delta F|^2$ ) and its observed mean over reflections ( $\overline{|\Delta F|^2}$ ):

$$w = \left( 1 + \frac{\sigma_{\Delta F}^2}{\overline{\sigma_{\Delta F}^2}} + \alpha \frac{|\Delta F|^2}{\overline{|\Delta F|^2}} \right)^{-1}. \quad (7)$$

With  $\alpha = 0$ , these weights take the form derived by Ursby & Bourgeois (1997). The  $\Delta F$ -dependent term downweights the

influence of likely outliers in the data set resulting from poorly measured differences by assigning lower weights to their map coefficients. The tolerance for large differences is controlled by the  $\alpha$  parameter.  $\alpha$  values of 1.0 (Šrajer *et al.*, 2001) and 0.05 (Hekstra *et al.*, 2016) have been reported in the literature.

The weighting function given by equation (7) can be expressed in a few lines of Python that apply weights based on the values of  $|\Delta F|$  and  $\sigma_{\Delta F}$  in an `rs.DataSet` object [Fig. 4(a)]. The weights computed for the PYP data set are illustrated in Fig. 4(b). Difference structure factors with low signal-to-noise ratios (large  $\sigma_{\Delta F}$  relative to  $|\Delta F|$ ) or large difference structure factor amplitudes are assigned lower weight. The unweighted and weighted difference maps were then made using phases derived from the ground-state model (PDB entry 2phy; Borgstahl *et al.*, 1995). The side-by-side comparison of these difference maps shows that the weights greatly improve the interpretability of the structural changes – emphasizing the *trans*-to-*cis* isomerization of the chromophore, as well as concerted changes in the nearby Arg52 and Phe96 side chains [Figs. 4(c) and 4(d)].

This example illustrates the use of *reciprocalspaceship* to create custom maps. Importantly, it demonstrates both the exploratory analysis of different weighting schemes and the

writing of MTZ files including different weight columns. These can be used to visualize the impact of the different weights in a molecular visualization suite.

#### 4. Discussion

*reciprocalspaceship* is a Python library that can form the foundation for the development of new methods in crystallographic data analysis. This library provides a `DataSet` object that can conveniently represent tabular reflection data while adhering to common practices in Python data analysis. This empowers crystallographers to write idiomatic Python code to analyze their experiments while having full support for the necessary features of crystallographic analysis, such as symmetry operations, unit cells and space groups. Example applications have been presented which use this library to merge scaled reflections, analyze anomalous differences from a SAD experiment and observe the impact of weights on a time-resolved difference map. These examples illustrate how *reciprocalspaceship* could be used in several different contexts, producing useful analyses

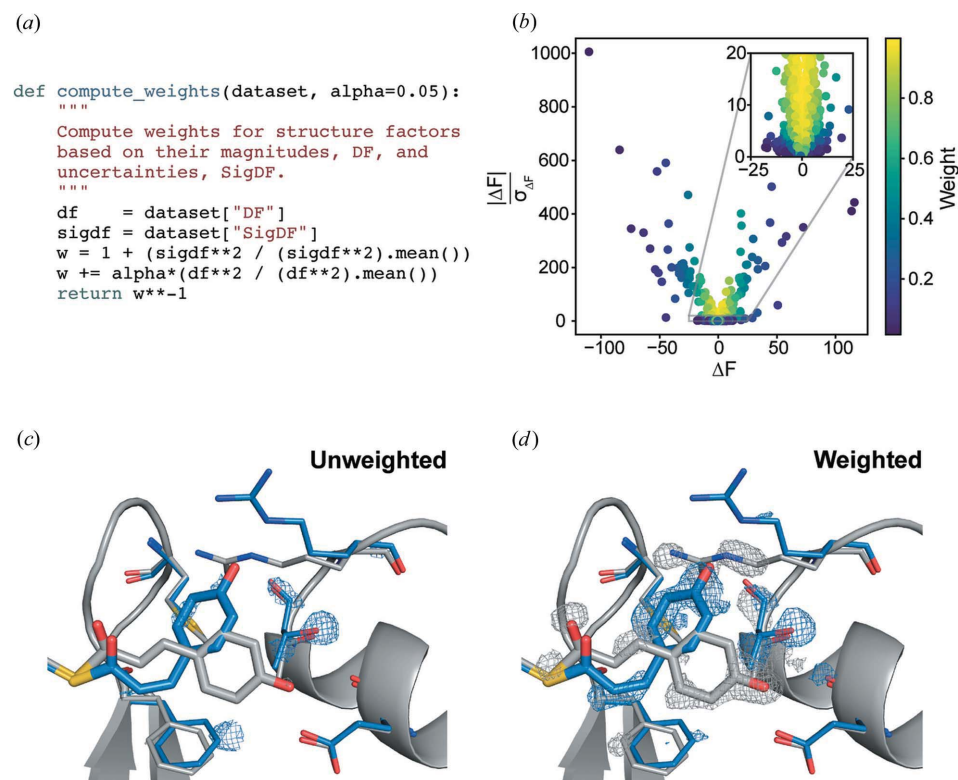


**Figure 4**

Weighting a time-resolved difference map. (a) The Python function for applying weights to arrays of difference structure factor amplitudes and uncertainties. (b) A scatter plot showing the weights assigned to each observed difference structure factor amplitude with  $\alpha = 0.05$ . (c) An unweighted  $|F_{\text{on}}| - |F_{\text{off}}|$  difference map in the vicinity of the PYP chromophore. (d) A weighted  $|F_{\text{on}}| - |F_{\text{off}}|$  difference map with  $\alpha = 0.05$ . The *trans* (ground state) PYP structure (gray) is taken from PDB entry 2phy and the *cis* (excited, pB state) PYP structure (blue) is taken from PDB entry 3ume (Tripathi *et al.*, 2012). The difference maps are contoured at  $\pm 3\sigma$  and were carved within 1.2 Å of the displayed residues. These figures were rendered using *PyMOL* (Schrödinger, 2020).



with relatively short scripts and functions that can take full advantage of the existing Python ecosystem.

*reciprocalspaceship* can be used for exploratory data analysis, allowing one to inspect interesting properties of an important data set. Or it can be used to prototype, develop and ship new methods and algorithms for analyzing data sets (Dalton *et al.*, 2021). Furthermore, this library can be useful in teaching crystallography by allowing students to familiarize themselves with reflection data, space groups and symmetry and the implementation of commonly used algorithms. By using a framework familiar to Python data scientists, this library lowers the barrier to entry for crystallographic software development.

## 5. Data and code availability

*reciprocalspaceship* and worked-out examples are available on GitHub at <https://github.com/Hekstra-Lab/reciprocalspaceship> and can be installed directly from *PyPI*. The complete code used in these examples is available in the *reciprocalspaceship* documentation, and the interactive Jupyter notebooks and all supporting data can be downloaded directly from the `Examples` directory of the GitHub repository.

## Acknowledgements

We thank the staff at the Northeastern Collaborative Access Team (NE-CAT), beamline 24-ID-C of the Advanced Photon Source, for supporting our room-temperature crystallography experiments, with special thanks to Igor Kourinov. We also thank Marius Schmidt and Vukica Šrajer for the time-resolved Laue diffraction data of photoactive yellow protein.

## Funding information

Funding for this research was provided by Searle Scholarship Program (scholarship No. SSP-2018-3240 to DRH); George W. Merck Fund of the New York Community Trust (fellowship No. 338034 to DRH); and National Science Foundation Graduate Research Fellowship (grant No. DGE1745303 to JBG). NE-CAT beamlines are supported by the National Institute of General Medical Sciences, NIH (grant No. P30 GM124165), using resources of the Advanced Photon Source, a US Department of Energy (DOE) Office of Science User Facility operated for the DOE Office of Science by Argonne National Laboratory under contract No. DE-AC02-06CH11357.

## References

Abadi, M., Agarwal, A., Barham, P., Brevdo, E., Chen, Z., Citro, C., Corrado, G. S., Davis, A., Dean, J., Devin, M., Ghemawat, S., Goodfellow, I., Harp, A., Irving, G., Isard, M., Jia, Y., Jozefowicz, R., Kaiser, L., Kudlur, M., Levenberg, J., Mané, D., Monga, R., Moore, S., Murray, D., Olah, C., Schuster, M., Shlens, J., Steiner, B., Sutskever, I., Talwar, K., Tucker, P., Vanhoucke, V., Vasudevan, V., Viégas, F., Vinyals, O., Warden, P., Wattenberg, M., Wicke, M., Yu, Y. & Zheng, X. (2015). *TensorFlow: Large-scale Machine Learning on Heterogeneous Systems*, <https://www.tensorflow.org/>.  
Abrahams, S. C. & Keve, E. T. (1971). *Acta Cryst.* **A27**, 157–165.

Adams, P. D., Afonine, P. V., Bunkóczy, G., Chen, V. B., Davis, I. W., Echols, N., Headd, J. J., Hung, L.-W., Kapral, G. J., Grosse-Kunstleve, R. W., McCoy, A. J., Moriarty, N. W., Oeffner, R., Read, R. J., Richardson, D. C., Richardson, J. S., Terwilliger, T. C. & Zwart, P. H. (2010). *Acta Cryst.* **D66**, 213–221.  
Borgstahl, G. E., Williams, D. R. & Getzoff, E. D. (1995). *Biochemistry*, **34**, 6278–6287.  
Cooley, J. W. & Tukey, J. W. (1965). *Math. Comput.* **19**, 297–301.  
Dalton, K. M., Greisman, J. B. & Hekstra, D. R. (2021). *bioRxiv*, <https://doi.org/10.1101/2021.01.05.425510>.  
Dods, R., Båth, P., Morozov, D., Gagné, V. A., Arnlund, D., Luk, H. L., Kübel, J., Maj, M., Vallejos, A., Wickstrand, C., Bosman, R., Beyerlein, K. R., Nelson, G., Liang, M., Milathianaki, D., Robinson, J., Harimoorthy, R., Berntsen, P., Malmerberg, E., Johansson, L., Andersson, R., Carbajo, S., Claesson, E., Conrad, C. E., Dahl, P., Hammarin, G., Hunter, M. S., Li, C., Lisova, S., Royant, A., Safari, C., Sharma, A., Williams, G. J., Yefanov, O., Westenhoff, S., Davidsson, J., DePonte, D. P., Boutet, S., Barty, A., Katona, G., Groenhof, G., Brändén, G. & Neutze, R. (2021). *Nature*, **589**, 310–314.  
Evans, P. R. & Murshudov, G. N. (2013). *Acta Cryst.* **D69**, 1204–1214.  
French, S. & Wilson, K. (1978). *Acta Cryst.* **A34**, 517–525.  
García-Bonete, M.-J. & Katona, G. (2019). *Acta Cryst.* **A75**, 851–860.  
Genick, U. K., Borgstahl, G. E. O., Ng, K., Ren, Z., Pradervand, C., Burke, P. M., Šrajer, V., Teng, T.-Y., Schildkamp, W., McRee, D. E., Moffat, K. & Getzoff, E. D. (1997). *Science*, **275**, 1471–1475.  
Greisman, J. B., Dalton, K. M. & Hekstra, D. R. (2021). Data Set for Hen Egg White Lysozyme by Native S-SAD at Room Temperature. Version 1.0.0. <https://doi.org/10.5281/zenodo.4426679>.  
Grosse-Kunstleve, R. W., Sauter, N. K., Moriarty, N. W. & Adams, P. D. (2002). *J. Appl. Cryst.* **35**, 126–136.  
Harris, C. R., Millman, K. J., van der Walt, S. J., Gommers, R., Virtanen, P., Cournapeau, D., Wieser, E., Taylor, J., Berg, S., Smith, N. J., Kern, R., Picus, M., Hoyer, S., van Kerkwijk, M. H., Brett, M., Haldane, A., del Río, J. F., Wiebe, M., Peterson, P., Gérard-Marchant, P., Sheppard, K., Reddy, T., Weckesser, W., Abbasi, H., Gohlke, C. & Oliphant, T. E. (2020). *Nature*, **585**, 357–362.  
Hatti, K. S., McCoy, A. J. & Read, R. J. (2021). *bioRxiv*, <https://doi.org/10.1101/2021.02.07.430107>.  
Hekstra, D. R., White, K. I., Socolich, M. A., Henning, R. W., Šrajer, V. & Ranganathan, R. (2016). *Nature*, **540**, 400–405.  
Howell, P. L. & Smith, G. D. (1992). *J. Appl. Cryst.* **25**, 81–86.  
Kabsch, W. (2010a). *Acta Cryst.* **D66**, 133–144.  
Kabsch, W. (2010b). *Acta Cryst.* **D66**, 125–132.  
Karplus, P. A. & Diederichs, K. (2012). *Science*, **336**, 1030–1033.  
Kluyver, T., Ragan-Kelley, B., Pérez, F., Granger, B., Bussonnier, M., Frederic, J., Kelley, K., Hamrick, J., Grout, J., Corlay, S., Ivanov, P., Avila, D., Abdalla, S., Willing, C. & Joint Development Team (2016). *Positioning and Power in Academic Publishing: Players, Agents and Agendas*, edited by F. Loizides & B. Schmidt, pp. 87–90. Amsterdam: IOS Press.  
Krekel, H., Oliveira, B., Pfannschmidt, R., Bruynooghe, F., Laughner, B. & Bruhin, F. (2020). *pytest*. Version 6.2.1. <https://github.com/pytest-dev/pytest>.  
Lange, K. L., Little, R. J. A. & Taylor, J. M. G. (1989). *J. Am. Stat. Assoc.* **84**, 881–896.  
Murphy, K. P. (2012). *Machine Learning: A Probabilistic Perspective*. Cambridge: MIT Press.  
Otwinski, Z. & Minor, W. (1997). *Methods in Enzymology*, Vol. 276, *Macromolecular Crystallography*, Part A, edited by C. W. Carter Jr & R. M. Sweet, pp. 307–326. New York: Academic Press.  
Paszke, A., Gross, S., Massa, F., Lerer, A., Bradbury, J., Chanan, G., Killeen, T., Lin, Z., Gimelshein, N., Antiga, L., Desmaison, A., Kopf, A., Yang, E., DeVito, Z., Raison, M., Tejani, A., Chilamkurthy, S., Steiner, B., Fang, L., Bai, J. & Chintala, S. (2019). *Advances in Neural Information Processing Systems*, Vol. 32, edited by H. Wallach, H. Larochelle, A. Beygelzimer, F.

- d'Alché-Buc, E. Fox & R. Garnett, pp. 8024–8035. Red Hook: Curran Associates.
- Reback, J., McKinney, W., Brockmendel, J., den Bossche, J. V., Augspurger, T., Cloud, P., Young, G. F., Hawkins, S., Sinhrks, Roeschke, M., Klein, A., Petersen, T., Tratner, J., She, C., Ayd, W., Naveh, S., Garcia, M., Schendel, J., Hayden, A., Saxton, D., Hofer, P., Jancauskas, V., McMaster, A., Battiston, P., Seabold, S., Gorelli, M., Dong, K. & Hoyer, S. (2021). *pandas*. Version 1.2.1. <https://doi.org/10.5281/zenodo.3509134>.
- Schrödinger (2020). *The pyMOL Molecular Graphics System*. Version 2.4. Schrödinger LLC, New York, USA.
- Šrajcar, V., Ren, Z., Teng, T.-Y., Schmidt, M., Ursby, T., Bourgeois, D., Pradervand, C., Schildkamp, W., Wulff, M. & Moffat, K. (2001). *Biochemistry*, **40**, 13802–13815.
- Terwilliger, T. C., Adams, P. D., Read, R. J., McCoy, A. J., Moriarty, N. W., Grosse-Kunstleve, R. W., Afonine, P. V., Zwart, P. H. & Hung, L.-W. (2009). *Acta Cryst.* **D65**, 582–601.
- Terwilliger, T. C., Bunkóczi, G., Hung, L.-W., Zwart, P. H., Smith, J. L., Akey, D. L. & Adams, P. D. (2016). *Acta Cryst.* **D72**, 359–374.
- Tripathi, S., Šrajcar, V., Purwar, N., Henning, R. & Schmidt, M. (2012). *Biophys. J.* **102**, 325–332.
- Ursby, T. & Bourgeois, D. (1997). *Acta Cryst.* **A53**, 564–575.
- Virtanen, P., Gommers, R., Oliphant, T. E., Haberland, M., Reddy, T., Cournapeau, D., Burovski, E., Peterson, P., Weckesser, W., Bright, J., van der Walt, S. J., Brett, M., Wilson, J., Millman, K. J., Mayorov, N., Nelson, A. R. J., Jones, E., Kern, R., Larson, E., Carey, C. J., Polat, İ., Feng, Y., Moore, E. W., VanderPlas, J., Laxalde, D., Perktold, J., Cimrman, R., Henriksen, I., Quintero, E. A., Harris, C. R., Archibald, A. M., Ribeiro, A. H., Pedregosa, F., van Mulbregt, P., Vijaykumar, A., Bardelli, A. P., Rothberg, A., Hilboll, A., Kloeckner, A., Scopatz, A., Lee, A., Rokem, A., Woods, C. N., Fulton, C., Masson, C., Hägström, C., Fitzgerald, C., Nicholson, D. A., Hagen, D. R., Pasechnik, D. V., Olivetti, E., Martin, E., Wieser, E., Silva, F., Lenders, F., Wilhelm, F., Young, G., Price, G. A., Ingold, G., Allen, G. E., Lee, G. R., Audren, H., Probst, I., Dietrich, J. P., Silterra, J., Webber, J. T., Slavič, J., Nothman, J., Buchner, J., Kulick, J., Schönberger, J. L., de Miranda Cardoso, J. V., Reimer, J., Harrington, J., Rodríguez, J. L. C., Nunez-Iglesias, J., Kuczynski, J., Tritz, K., Thoma, M., Neville, M., Kümmerer, M., Bolingbroke, M., Tartre, M., Pak, M., Smith, N. J., Nowaczyk, N., Shebanov, N., Pavlyk, O., Brodtkorb, P. A., Lee, P., McGibbon, R. T., Feldbauer, R., Lewis, S., Tygier, S., Sievert, S., Vigna, S., Peterson, S., More, S., Pudlik, T., Oshima, T., Pingel, T. J., Robitaille, T. P., Spura, T., Jones, T. R., Cera, T., Leslie, T., Zito, T., Krauss, T., Upadhyay, U., Halchenko, Y. O. & Vázquez-Baeza, Y. (2020). *Nat. Methods*, **17**, 261–272.
- Walt, S. van der, Schönberger, J. L., Nunez-Iglesias, J., Boulogne, F., Warner, J. D., Yager, N., Gouillart, E., Yu, T. & The scikit-image Contributors (2014). *PeerJ*, **2**, e453.
- Weiss, M. S. (2001). *J. Appl. Cryst.* **34**, 130–135.
- Wickstrand, C., Katona, G., Nakane, T., Nogly, P., Standfuss, J., Nango, E. & Neutze, R. (2020). *Struct. Dyn.* **7**, 024701.
- Wilson, A. J. C. (1949). *Acta Cryst.* **2**, 318–321.
- Winn, M. D., Ballard, C. C., Cowtan, K. D., Dodson, E. J., Emsley, P., Evans, P. R., Keegan, R. M., Krissinel, E. B., Leslie, A. G. W., McCoy, A., McNicholas, S. J., Murshudov, G. N., Pannu, N. S., Potterton, E. A., Powell, H. R., Read, R. J., Vagin, A. & Wilson, K. S. (2011). *Acta Cryst.* **D67**, 235–242.
- Winter, G., Waterman, D. G., Parkhurst, J. M., Brewster, A. S., Gildea, R. J., Gerstel, M., Fuentes-Montero, L., Vollmar, M., Michels-Clark, T., Young, I. D., Sauter, N. K. & Evans, G. (2018). *Acta Cryst.* **D74**, 85–97.
- Wojdyr, M. (2021). *GEMMI – A Library for Structural Biology*, <https://github.com/project-gemmi/gemmi>.